Terahertz-field-induced second harmonic generation through Pockels effect in zinc telluride crystal

Marion Cornet, Jérôme Degert, Emmanuel Abraham, Eric Freysz

Terahertz-field-induced second harmonic generation through Pockels effect in zinc telluride crystal

Marion Cornet,[1,2] Jérôme Degert,[1,2] Emmanuel Abraham,[1,2] and Eric Freysz[1,2,*]

[1]*Univ. Bordeaux, LOMA, UMR 5798, F-33400 Talence, France*

[2]*CNRS, LOMA, UMR 5798, F-33400 Talence, France*

**Corresponding author: e.freysz@loma.u-bordeaux1.fr*

Received September 1, 2014; revised September 15, 2014; accepted September 16, 2014; posted September 16, 2014 (Doc. ID 222284); published October 10, 2014

We report on the second harmonic generation (SHG) of a near-infrared pulse in a zinc telluride crystal through the Pockels effect induced by an intense terahertz pulse. The temporal and angular behaviors of the SHG have been measured and agree well with theoretical predictions. This phenomenon, so far overlooked, makes it possible to generate second harmonic through cascading of two second-order nonlinear phenomena in the near-infrared and terahertz ranges. We also show how this cascading process can be used to sample terahertz pulses.

OCIS codes: (190.0190) Nonlinear optics; (320.0320) Ultrafast optics; (190.2620) Harmonic generation and mixing.
http://dx.doi.org/10.1364/OL.39.005921

Second harmonic generation (SHG) or frequency doubling can be considered to be one of the most widely used nonlinear optical processes. It was first demonstrated in 1961 thanks to the invention of the laser providing the required high intensity monochromatic light [1]. SHG has also been recorded in centrosymmetric media immersed in a DC or an AC electric field. The electric field breaks the centrosymmetry of the medium giving it the ability to generate second harmonic [2]. Electric-field-induced second harmonic (EFISH) has been reported in a large variety of media [3–5]. For a while, these measurements were restricted to low frequency AC fields. However, thanks to the recent developments of intense pulsed sources in the terahertz (THz) range [6,7], THz-field-induced SHG (TFISH) has been reported in beta barium borate crystal [8] and in many centrosymmetric media [9–11]. TFISH can be described as a third-order nonlinear phenomenon in which the signal intensity is proportional to the THz intensity I_{THz}, the square of the fundamental laser intensity I_ω, and the third-order susceptibility $\chi^{(3)}$ of the material: $I_{2\omega}^{\mathrm{TFISH}} \sim |\chi^{(3)}|^2 I_\omega^2 I_{\mathrm{THz}}$. However, one should mention that the frontier between second-order and third-order nonlinear optical phenomena is not strict. In the early stage of nonlinear optics, it was recognized that second-order phenomena could effectively contribute to third-order-like nonlinearities through a cascading of two second-order processes [12]. Many experiments showed that during SHG such a cascading can result in very large third-order-like nonlinearities that open a wide range of applications [13].

In this Letter, we analyze cascading of two second-order nonlinear phenomena in the THz and near-IR (NIR) spectral range. We will refer to this, which has so far been overlooked, as Pockels effect (PE)-Induced Second Harmonic (PISH). It occurs during the interaction between a THz and an optical pulse in a noncentrosymmetric medium. This phenomenon is demonstrated in a zinc telluride (ZnTe) crystal that is widely used in the THz range because of its second-order nonlinear optical properties [14]. This crystal is expected to exhibit both second-order [PE or SHG] and third-order (TFISH) nonlinear processes. We will demonstrate that the SHG signal, $I_{2\omega}^{\mathrm{PISH}}$, resulting from cascading of two second-order processes (namely PE and SHG) overcomes the signal produced by TFISH. Finally, we will show that this cascading process is also an efficient means to sample the THz pulse.

The experimental setup is displayed in Fig. 1. An amplified Ti:sapphire regenerative amplifier yields, at 1 kHz repetition rate, 1.5 mJ pulses centered at 800 nm having a 60 fs duration. The laser beam is split into pump and probe beams for THz generation and SHG, respectively. The pump beam is sent onto a holographic grating (1800 grooves/mm) that introduces a given pulse front tilt satisfying the phase matching condition for optical rectification in a stochiometric $LiNbO_3$ crystal. Appropriate tilt angle and grating imaging into the crystal are controlled by two lenses. The pump beam is slightly focused onto the crystal. One surface of the crystal is cut with the phase matching angle of 62°. THz pulses with 20 kV/cm electric field strength are generated from the crystal, covering the 0.1–3 THz spectral range. The $\hat{y}$-polarized THz beam is focused onto the ZnTe crystal with a pair of off-axis parabolic mirrors. A delay stage makes it

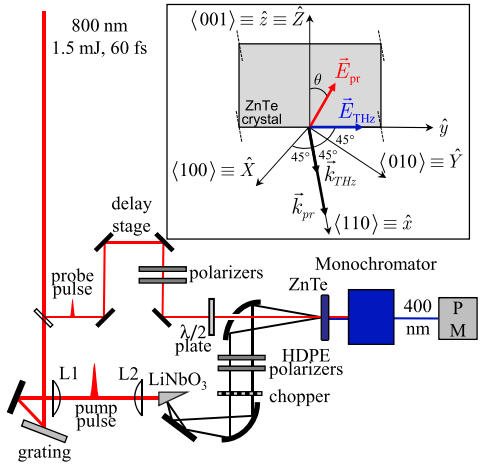

Fig. 1. Experimental setup: PM, photomultiplier tube. Inset: geometry of the experiment. $(\hat{X}, \hat{Y}, \hat{Z})$, cartesian frame of the crystal; $(\hat{x}, \hat{y}, \hat{z})$, cartesian frame of the laboratory.

possible to delay the probe pulse with respect to the THz pump pulse. Finally, THz and IR probe intensities can be adjusted by a set of polarizers. For the calibration of the THz field, we used the known electro-optic coefficient of ZnTe. For the detection of the second-harmonic (SH) signal we used a photomultiplier tube recording the output of a monochromator centered at 400 nm and an optical chopper connected to a lock-in amplifier.

At first, we investigated the TFISH generation in a ⟨100⟩ cut 300-μm-thick ZnTe crystal. For such a crystal cut, and owing to the symmetry of this crystal, second-order nonlinear effects such as direct SHG or PE are not possible. However, upon the application of a THz field, SHG induced by TFISH is expected. The THz and probe pulses, linearly and cross-polarized, were collinearly propagating in the crystal. Under these experimental conditions and whatever the rotation of the crystal around the ⟨100⟩ axis, no TFISH signal was recorded. This means that, with our detection, the used fundamental fluence and THz field strength of ∼20 kV/cm make it impossible to reveal the TFISH phenomenon in ZnTe. This is at variance with a previous study where the observation of TFISH was easily recorded using a BBO crystal and similar THz electric field strength [8]. However, in this later study, the BBO crystal cut was not preventing second-order nonlinear effects, and the assignment of the signal to TFISH instead of a cascading of second-order processes is questionable. To address this question properly, we performed a similar experiment in a ⟨110⟩ cut 300-μm-thick ZnTe crystal. For such cut, the crystal could exhibit both PE and SHG. Inside the crystal, the THz beam and the probe beam propagate collinearly along the ⟨110⟩ axis [Fig. 1(b)]. A half-wave plate is employed to linearly polarize the probe beam at the angle θ with respect to the ⟨001⟩ axis. Owing to the crystal symmetry, when $\theta = 0°$ or 180° no SHG is produced in the crystal. We first investigated the intensity dependence of the SHG signal for $\theta = 0°$. As expected, without the THz pulse, no SHG was recorded. Then, performing the same experiment in the presence of the THz pulse, the SHG was easily observed. This signal was only recorded when the fundamental and THz pulses were temporarily overlapping within the crystal. It disappears if the monochromator is set 20 nm above or below 400 nm. This observation is surprising. Indeed, if one neglects cascading of second-order processes, only TFISH takes place for $\theta = 0°$. However, according to our previous experiment, this process cannot be recorded by our detection system. The evolution and the fit of this SHG signal with respect to I_ω and I_{THz} are displayed in Fig. 2. Note that this dependence is strictly similar to the intensity dependence expected for a TFISH signal. To discriminate the TFISH and PISH contribution to SHG, we investigated the dependence of the SHG signal as a function of the angle θ between the probe beam polarization and the ⟨001⟩ axis of the crystal. The angular dependence of the direct SHG signal measured in the absence of the THz pulse is represented by the black squares in Fig. 3. In the presence of the THz pulse and modulating only the THz pulse, we could suppress this direct SHG signal with the lock-in detection. The SHG signal recorded upon application of the THz field is represented by the red circles in Fig. 3. In agreement with

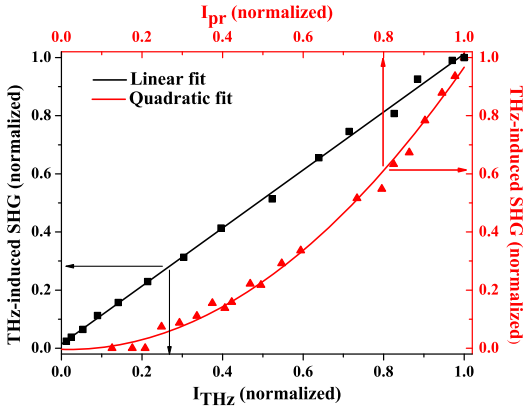

Fig. 2. Peak value of the THz-field-induced SHG signal with respect to the THz intensity I_{THz} [(■) linked to the bottom and left axis] and to the probe intensity I_ω [(▲) linked top and right axis] for $\theta = 0°$. The red (resp. black) solid curve corresponds to a quadratic (resp. linear) fit of the data.

the angular dependence of PE in this crystal, it is maximum at $\theta = 0°$ and almost null at $\theta = 45°$ [14]. This SHG signal may be negative, revealing a π phase-shift of the lock-in amplifier. This ensemble of data clearly indicates that the SHG signal likely results from a cascading of second-order nonlinear processes, namely PE and SHG. These two second-order nonlinear effects are combined as follows: as the THz pulse propagates through the crystal, it induces PE that rotates the polarization of the fundamental pulse, enabling it to be frequency-doubled by the intrinsic second-order nonlinearity of the crystal.

To model this phenomenon, let us consider the probe and THz fields as nondepleted plane waves, propagating along the x axis, expressed as $E_{\mathrm{pr}}(t,x) = \frac{1}{2}\mathcal{E}^{\omega}(x)e^{-i(\omega t - k_\omega x)} + \mathrm{c.c}$ and $E_{\mathrm{THz}}(t,x) = \frac{1}{2}E_{\mathrm{THz}}e^{-i(\Omega t - k_\Omega x)} + \mathrm{c.c.}$, respectively. In these expressions, c.c. denotes the complex conjugate, $k_\omega = \frac{n_\omega \omega}{c}$, $k_\Omega = \frac{n_\Omega \Omega}{c}$, and n_ω and n_Ω are the refractive indices of the crystal at the probe and THz frequencies, respectively. As depicted in the inset of Fig. 1, at the entrance of the crystal in the frame of the laboratory, the probe field amplitude is expressed as $(\mathcal{E}_x^{\omega,\mathrm{in}} = 0, \mathcal{E}_y^{\omega,\mathrm{in}} = E_{\mathrm{pr}} \sin\theta, \mathcal{E}_z^{\omega,\mathrm{in}} = E_{\mathrm{pr}} \cos\theta)$.

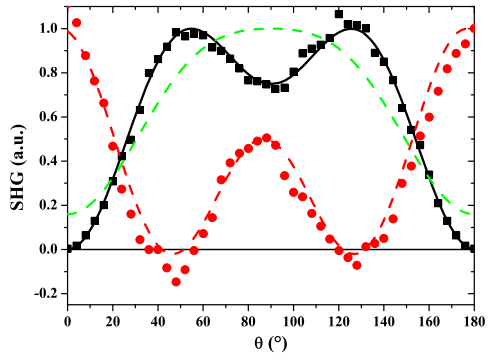

Fig. 3. Angular dependence of the peak value of the SHG signal. (■) SHG recorded when the probe beam is modulated and $E_{\mathrm{THz}} = 0$. (•) SHG recorded when the THz pump beam is modulated and $E_{\mathrm{THz}} \neq 0$. The solid black and dashed red curves correspond to a normalized plot of Eqs. (3). The green dashed curve corresponds to a normalized plot of the TFISH angular dependence.

Then, the PE induced by the THz pump in the crystal alters the polarization state of the NIR probe pulse. In the frame of the crystal, the probe field amplitude at each point x of the crystal is given by:

$$\mathcal{E}_X^{\omega,c} = -\frac{E_{\mathrm{pr}}}{2}[\cos(\psi)e^{i\Gamma x} - \sin(\psi)e^{-i\Gamma x}], \tag{1a}$$

$$\mathcal{E}_Y^{\omega,c} = -\mathcal{E}_X^{\omega,c}, \tag{1b}$$

$$\mathcal{E}_Z^{\omega,c} = \frac{E_{\mathrm{pr}}}{\sqrt{2}}[\cos(\psi)e^{i\Gamma x} + \sin(\psi)e^{-i\Gamma x}], \tag{1c}$$

with $\psi = \pi/4 - \theta$, $\Gamma = (\pi/\lambda)n_\omega^3 r_{41}E_{\mathrm{THz}}$ [14], where r_{41} is the electro-optic coefficient of the crystal and λ the wavelength of the probe. In the frame of the crystal, the slowly varying amplitude of the second-order polarization at 2ω is given by [15]: $\mathcal{P}_i^{(2)} = \varepsilon_0\chi_{ijk}^{(2)}\mathcal{E}_j^{\omega,c}\mathcal{E}_k^{\omega,c}$, where $i \neq j \neq k = X,Y,Z$ and $\chi_{XYZ}^{(2)} = \chi_{YZX}^{(2)} = \chi_{ZXY}^{(2)} = \chi^{(2)}$ is the second-order susceptibility of the crystal. The field radiated by these nonlinear polarization components can be computed solving the nonlinear wave equation. In the slowly varying amplitude approximation and introducing the absorption $\alpha_{2\omega}$ of the SH field by the crystal it is expressed as $(\frac{\partial}{\partial x} + \alpha_{2\omega})\mathcal{E}_\ell^{2\omega} = \frac{i\omega}{n_{2\omega}c\varepsilon_0}\mathcal{P}_\ell^{(2)}\exp(i\Delta k x)$ $(\ell = y,z)$, where $\Delta k = 2\omega(n_\omega - n_{2\omega})/c$ are the absorption coefficient and the phase mismatch between the fundamental and SH fields, respectively. When $\Gamma \ll \Delta k$, $\Gamma x \ll 1$ and $\alpha_{2\omega}x \gg 1$, the resolution of this latter equation with the boundary condition $\mathcal{E}_{y,z}^{2\omega}(x=0) = 0$ yields to

$$\mathcal{E}_{y,z}^{2\omega}(x) = -iA\exp(i\Delta k x)g_{y,z}(\Gamma x,\psi), \tag{2}$$

where

$$A = \omega\chi^{(2)}E_{\mathrm{pr}}^2/(2cn_{2\omega}(i\Delta k + \alpha_{2\omega}))$$

and

$$g_y(\Gamma x,\psi) \simeq (1 + 2i\Gamma x - 2\Gamma^2x^2)\cos^2(\psi) - (1 - 2i\Gamma x - 2\Gamma^2x^2)\sin^2(\psi), \tag{3a}$$

$$g_z(\Gamma x,\psi) \simeq \left[\left(1 + i\Gamma x - \frac{\Gamma^2x^2}{2}\right)\cos(\psi) - \left(1 - i\Gamma x - \frac{\Gamma^2x^2}{2}\right)\sin(\psi)\right]^2. \tag{3b}$$

Notice that $\alpha_{2\omega}x \gg 1$ at the exit of a 300-μm-thick crystal since, in ZnTe, $\alpha_{2\omega} \simeq 1.25\ \mu\mathrm{m}^{-1}$ at 400 nm [16]. These expressions exhibit the SH field, $\mathcal{E}^0$, corresponding to the intrinsic SHG of the crystal, that is proportional to A (i.e., $\mathcal{E}^0 \sim \chi^{(2)}E_{\mathrm{pr}}^2$) as well as the SH field, $\mathcal{E}^{\mathrm{PISH}}$, induced by PE that is phase shifted by $\pi/2$ and proportional to $A\Gamma x$ (i.e., $\mathcal{E}^{\mathrm{PISH}} \sim \chi^{(2)}r_{41}E_{\mathrm{pr}}^2E_{\mathrm{THz}}x/\lambda$). We have also computed the slowly varying amplitude of the polarization giving rise to TFISH:

$$\mathcal{P}_y^{(3)}(x) = -\frac{3}{2}\varepsilon_0E_{\mathrm{pr}}^2E_{\mathrm{THz}}\left[\frac{1}{2}(a+b)\sin^2\theta + b\right], \tag{4a}$$

$$\mathcal{P}_z^{(3)}(x) = \frac{3}{2}\varepsilon_0E_{\mathrm{pr}}^2E_{\mathrm{THz}}b\sin^2\theta, \tag{4b}$$

where $a = \chi_{iiii}^{(3)}$ and $b = \chi_{iijj}^{(3)} = \chi_{ijij}^{(3)}$ are the two independent third-order susceptibility components of the crystal $(i,j = X,Y,Z)$. When $\alpha_{2\omega}x \gg 1$, the integration of the nonlinear wave equation with these nonlinear polarization components using the boundary condition $\mathcal{E}_{y,z}^{\mathrm{TFISH}}(x=0) = 0$ yields to

$$\mathcal{E}_y^{\mathrm{TFISH}}(x) = -iB\exp(i\Delta k x)\left[\frac{1}{2}(1+u)\sin^2\theta + 1\right], \tag{5a}$$

$$\mathcal{E}_z^{\mathrm{TFISH}}(x) = -iB\exp(i\Delta k x)\sin(2\theta), \tag{5b}$$

where $B = 3\omega\chi_{XXYY}^{(3)}E_{\mathrm{pr}}^2E_{\mathrm{THz}}/(2cn_{2\omega}(i\Delta k + \alpha_{2\omega}))$ and $u = a/b$. As expected, the TFISH field is proportional to $\chi_{XXYY}^{(3)}E_{\mathrm{pr}}^2E_{\mathrm{THz}}$. Equations (2)–(5) make it possible to compare the amplitudes and angular dependencies of the different contributions to SHG. At first, they are all found to have the same dependencies with respect to Δk. Note that, owing to the natural dispersion of the ZnTe crystal, $n_\omega \neq n_{2\omega}$ and $\Delta k \neq 0$. Second, the angular dependencies of the SH signal proportional to $|\mathcal{E}_y|^2 + |\mathcal{E}_z|^2$, can be easily computed. In Fig. 3, we have plotted the angular dependencies of the natural SHG, PISH, and TFISH. When $\Gamma x \ll 1$, and taking into account that $a = 2b$ [17], they are found to vary as $\sin^2(2\theta) + \sin^4(\theta)$, $2 - 10\cos^2(\theta) + 12\cos^4(\theta)$, and $(3/2\sin^2(\theta) + 1)^2 + \sin^2(2\theta)$, respectively. We have a good agreement between experiment and theory for the natural SHG and the PISH signal. However, one may wonder why we could not detect the TFISH signal. To address this question, we have computed the ratio $R = (A\Gamma L/B)^2 = (\pi\chi_{XYZ}^{(2)}r_{41}n_\omega^3L/(3\chi_{XXYY}^{(3)}\lambda))^2$ between the prefactor in front of the PISH and TFISH signals. This ratio depends on the ratio between the second and third-order nonlinear coefficients (i.e., $(\chi_{XYZ}^{(2)}r_{41}/\chi_{XXYY}^{(3)})^2$) as well as the ratio $(L/\lambda)^2$; hence the longer the crystal, the larger the ratio. At the exit of the 300-μm-thick crystal and considering that for ZnTe: $\chi_{XXYY}^{(3)} = 2.5\times10^{-19}\ \mathrm{m}^2\cdot\mathrm{V}^{-2}$, $r_{41} = 3.9\times10^{-12}\ \mathrm{m}\cdot\mathrm{V}^{-1}$, $n_\omega = 2.9$, $\chi_{XYZ}^{(2)} = 1\times10^{-10}\ \mathrm{m}\cdot\mathrm{V}^{-1}$, $L = 300\ \mu\mathrm{m}$ and $\lambda = 0.8\ \mu\mathrm{m}$, we found $R \approx 220$ [14,17]. In good agreement with our experimental data, this ratio indicates that TFISH may only contribute to SHG when crystal orientation minimizes the PISH contribution (i.e., $\theta = 45°$ or $135°$). Our computation was made considering continuous waves; its extension considering pulse propagation is straightforward if, as expected for such a thin crystal, one neglects the group velocity mismatch between THz and probe pulses in the crystal. In this case, the intensity of the SH pulse can be computed considering a steady state THz field and summing the SH intensity produced by each spectral components of the probe pulse [5]. Consequently, the amplitude of the SH

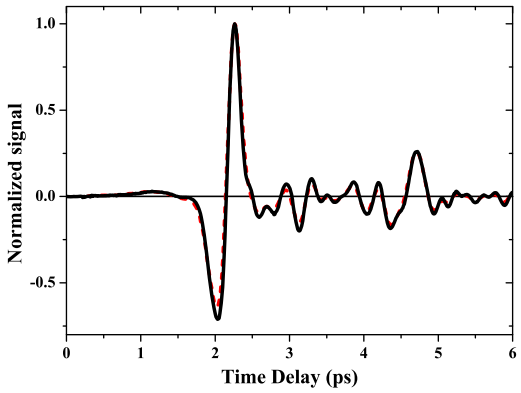

Fig. 4. Electro-optic signal measured with a balanced detection (dashed red curve) and heterodyned PISH signal difference for $\theta = 0°$ and $\alpha = 10°$ (black curve), as a function of the time delay between the IR probe and the THz pump pulses.

signal will increase but its angular dependence will remain unchanged.

According to our analysis, the PISH signal is proportional to the square of the THz electric field. Therefore, it could be interesting to adopt here an heterodyne detection to record directly the temporal evolution of the THz electric field [8]. However, as already mentioned, PISH and natural SHG signals are phase shifted by $\pi/2$ and cannot interfere. To overcome this problem, one can simply insert a quarter-wave plate on the probe beam pathway in front of the crystal. Let us call α the angle between the fast axis direction of the plate and the $\langle 001 \rangle$ axis of the crystal corresponding to the orientation of the probe beam polarization. It can be shown that during its propagation in the crystal, the elliptical probe beam will now also produce a SHG component proportional to α that will be phase shifted by $\pi/2$. The interference of the latter SHG component with the PISH signal can now be used to perform an heterodyne detection. Then, by successively measuring the heterodyned PISH signal for α and $-\alpha$, one can compute the following quantity $S_{2\omega}(\alpha) - S_{2\omega}(-\alpha) \sim 2\frac{L}{\lambda}\alpha\chi^{(2)}r_{41}I_{\mathrm{pr}}E_{\mathrm{THz}}$, that is directly proportional to the THz electric field. The experimental result is presented in Fig. 4 for $\alpha = 10°$ and compared with the electro-optic signal measured with an ellipsometer consisting in a quarter-wave plate combined with a Wollaston prism, followed by two balanced photodiodes connected to a lock-in amplifier for detection. The similarity of both signals is excellent which demonstrates the proportionality of the heterodyned PISH signal to the THz electric field. The signal to noise ratio of both signals is similar, demonstrating that the PISH effect can be an interesting and simple means to sample THz temporal waveforms.

To summarize, we have observed a THz-field-induced SHG in a zinc telluride crystal. Thanks to the measurements of the angular, intensity, and temporal dependencies of the signal and the theoretical analysis of our experiment, we have demonstrated that this SHG signal is because of the cascading of two second-order nonlinear processes, with one of them in the THz range. This phenomena has also be recorded in another Zinc blende crystal [18].

References

1. P. Franken, A. Hill, C. Peters, and G. Weinreich, Phys. Rev. Lett. **7**, 118 (1961).
2. R. W. Terhune, P. D. Maker, and C. M. Savage, Phys. Rev. Lett. **8**, 404 (1962).
3. G. Mayer, C.R. Acad. Sci. **267B**, 54 (1968).
4. P. M. Blanchard and G. R. Mitchell, Appl. Phys. Lett. **63**, 2038 (1993).
5. H. Guillet de Chatellus and E. Freysz, Opt. Express **9**, 586 (2001).
6. J. Hebling, G. Almasi, I. Z. Kozma, and J. Kuhl, Opt. Express **10**, 1161 (2002).
7. H. Hirori, A. Doi, F. Blanchard, and T. Tanaka, Appl. Phys. Lett. **98**, 091106 (2011).
8. J. Chen and X.-C. Zhang, Appl. Phys. Lett. **95**, 011118 (2009).
9. J. Dai, X. Xie, and X.-C. Zhang, Phys. Rev. Lett. **97**, 103903 (2006).
10. A. Nahata and T. Heinz, Opt. Lett. **23**, 67 (1998).
11. D. J. Cook, J. X. Chen, E. A. Morlino, and H. M. Hochstrasser, Chem. Phys. Lett. **309**, 221 (1999).
12. L. A. Ostrovskii, JETP Lett. **5**, 272 (1967).
13. G. I. Stegeman, D. J. Hagan, and L. Torner, Opt. Quantum Electron. **28**, 1691 (1996).
14. P. C. M. Planken, H.-K. Nienhuys, H. J. Bakker, and T. Wenckebach, J. Opt. Soc. Am. B **18**, 313 (2001).
15. P. N. Butcher and D. Cotter, *The Elements of Nonlinear Optics* (Cambridge University, 1991).
16. M. Cardona, J. Appl. Phys. **36**, 2181 (1965).
17. J. P. Caumes, L. Videau, C. Rouyer, and E. Freysz, Phys. Rev. Lett. **89**, 047401 (2002).
18. M. Cornet, A. Ould Hamouda, J. Degert, E. Abraham, and E. Freysz, in *CLEO: QELS Fundamental Science (CLEO QELS)* (Optical Society of America, 2014) paper FTu3D.2.